AIAA JOURNAL
Vol. 38, No. 2, February 2000

Separated Flow Surface Pressure Fluctuations and Pressure–Velocity Correlations on Prolate Spheroid

Michael C. Goody,* Roger L Simpson,† and Christopher J. Chesnakas‡
Virginia Polytechnic Institute and State University, Blacksburg, Virginia 24061-0203

Power spectra of turbulent surface pressure fluctuations and spatial correlation coefficients of surface pressure–velocity are presented for the leeside, three-dimensional, separated crossflow over a 6:1 prolate spheroid at $Re_L = 4.2 \times 10^6$ for angles of attack of 10 and 20 deg. This is a complex, three-dimensional, nonequilibrium flow of practical interest. These results are related to the attached, separated, and reattached features of the vortical flow for a range of Reynolds numbers based on momentum thickness up to 1.5×10^4. The high-frequency surface pressure fluctuation spectra scale on wall variables at low angle of attack. Near regions of separation where wall shear stress is low, there is little high-frequency content, whereas low-frequency contributions from the outer layer are relatively large. In regions with large surface shearing stresses, the wall region produces strong, high-frequency spectral content. At locations with relatively small outer region mean velocity gradients, there are smaller low-frequency contributions. Both of these features occur around the side of the body and under the large vortices at higher angle of attack. Therefore, at these locations spectral values are nearly constant at middle frequencies. The resulting rms pressure fluctuation distributions over the surface reflect the importance of the high-frequency wall region contributions. Around regions of boundary-layer separation there are local minima in rms pressure fluctuations, whereas around reattachments and under the large vortices there are local maxima in rms pressure fluctuations.

Nomenclature

d = pressure transducer sensing diameter, m
d_{local} = model diameter at a given axial position, m
d^+ = pressure transducer sensing diameter nondimensionalized on viscous scales, $u_\tau d/\nu$
L = model length, 1.37 m
p = pressure fluctuation at the model surface, Pa
Q_∞ = dynamic pressure of flow far upstream of model, $\frac{1}{2}\rho U_\infty^2$, Pa
q_e = dynamic pressure at edge of shear layer, $\frac{1}{2}\rho U_e^2$, Pa
R_{pv} = correlation coefficient of wall pressure and the fluctuating v component of velocity: $\overline{pv}/\sqrt{p^2}\sqrt{v^2}$
Re_L = model length Reynolds number, $U_\infty L/\nu$
Re_θ = momentum thickness Reynolds number, $U_\infty \theta/\nu$
r = distance from model surface along a line perpendicular to the model axis, m
r_S = distance between a point on the surface where pressure fluctuations are measured and the point in the flow that is the source of the pressure fluctuations, m
U = velocity component in a plane parallel to the surface, in the axial direction, m/s
U_C = convection velocity of pressure fluctuations, m/s
U_e = total velocity at edge of shear layer, m/s
U_∞ = wind-tunnel freestream velocity, m/s
u, v, w = fluctuating velocity components in the directions of U, V, and W, respectively, m/s
u_τ = friction velocity, $(\tau_W/\rho)^{1/2}$, m/s
V = mean velocity component normal to the local model surface, m/s
W = mean velocity component in a plane parallel to the local model surface and perpendicular to the axial direction (positive in $-\phi$ direction), m/s
x = axial distance from the nose of the model, m
y^+ = ru_τ/ν
α = angle of attack of model relative to incoming flow, deg
δ^* = boundary-layer displacement thickness, m

$$\int_0^\delta \left[1 - \frac{(U^2+W^2)^{\frac{1}{2}}}{(U^2+W^2)_e^{\frac{1}{2}}}\right] \mathrm{d}r$$

θ = boundary-layer momentum thickness, m

$$\int_0^\delta \left[1 - \frac{(U^2+W^2)^{\frac{1}{2}}}{(U^2+W^2)_e^{\frac{1}{2}}}\right]\left[\frac{(U^2+W^2)^{\frac{1}{2}}}{(U^2+W^2)_e^{\frac{1}{2}}}\right] \mathrm{d}r$$

ν = kinematic viscosity of fluid, m^2/s
ρ = mass density of flow, kg/m^3
τ_W = shear-stress magnitude at surface of model, Pa
Φ = power spectrum of surface pressure fluctuations ($Pa^2 \cdot s$) such that

$$\overline{p^2} = \int_0^\infty \Phi(\omega)\, \mathrm{d}\omega$$

ϕ = circumferencial angle coordinate, from windward side, deg
ω = circular frequency, rad/s

Superscript

$'$ = root mean square value of a fluctuating quantity

Presented as Paper 97-0485 at the AIAA 35th Aerospace Sciences Meeting, Reno, NV, 6–9 January 1997; received 15 July 1998; revision received 4 July 1999; accepted for publication 13 July 1999.

*Graduate Assistant, Department of Aerospace and Ocean Engineering, 215 Randolph Hall. Student Member AIAA.
†Jack E. Cowling Professor, Department of Aerospace and Ocean Engineering, 215 Randolph Hall. Fellow AIAA.
‡Research Associate, Department of Aerospace and Ocean Engineering; currently Mechanical Engineer, U.S. Naval Surface Warfare Center, Carderock Division, Code 5400, 9500 MacArthur Boulevard, West Bethesda, MD 20817-5700. Member AIAA.

I. Introduction

THE pressure fluctuations in a three-dimensional turbulent shear flow on a body, particularly in regions where the flow has separated, are a source of considerable noise and vibration. Though common, the sources of p are not well understood and are difficult to model. An increased understanding of the physics of this flowfield may improve the calculation, and perhaps control, of the noise generated by undersea vehicles and the handling characteristics of aircraft at high angle of attack.

The flow about a 6:1 prolate spheroid exhibits open separation phenomena of three-dimensional flow (Fig. 1). It is reflected by the

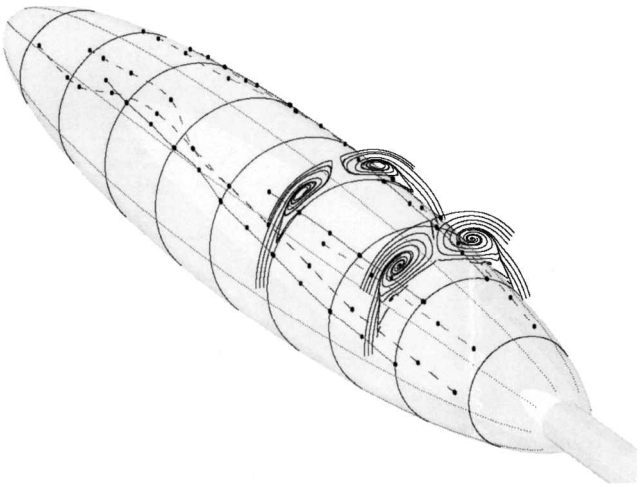

Fig. 1 Mean secondary flow about a 6:1 prolate spheroid at $\alpha = 20$ deg and $x/L = 0.600$ and 0.772 (see Ref. 15); solid lines on model surface show separation lines[1] as indicated by oil-flow visualization, dashed lines show minima in skin friction magnitude (Fig. 1 of Wetzel et al.[1]).

convergence of skin-friction lines.[1] The flow separating from the leeside rolls up into a strong vortex on each side of the body. This primary vortex may be accompanied by one or more smaller vortices, each of which is associated with a separation and reattachment line. The complex interactions between vortices result in a highly skewed, three-dimensional shear layer. Kreplin et al.,[2] Kreplin and Stäger,[3] Meier et al.,[4,5] and Vollmers et al.[6] have documented the surface flow, mean surface pressure, skin friction, and mean velocity at several Reynolds numbers and angles of attack. The leeside flow has proven difficult for turbulence models to calculate.[7–10]

The current study is part of an ongoing effort to extensively measure this flowfield to increase the understanding of the flow physics and to provide an experimental database for comparison with computations. The effects of Reynolds number and angle of attack on boundary-layer transition and separation location were studied by Ahn and Simpson.[11] Barber and Simpson[12] documented the mean and turbulent velocities in the crossflow separation region, but the use of five-hole pressure probes and crossed hot wires precluded them from obtaining data within the inner boundary layer. Previous studies of a tripped flow at a length Reynolds number $Re_L = 4.2 \times 10^6$ by Chesnakas and Simpson[7,13–15] did not suffer this limitation and have documented the turbulence structure, including all Reynolds stresses and velocity triple products, from y^+ closer than 7. This was possible through the use of the specially designed, miniature fiber-optic laser Doppler velocimetry (LDV) probe described in Chesnakas and Simpson.[14] Simpson[16–18] reviewed three-dimensional turbulent separation in detail. Wetzel et al.[1] focused on the measurement and quantitative description of three-dimensional crossflow separation.

Most fundamental experimental investigations of p beneath a turbulent boundary layer have been confined to equilibrium, or near-equilibrium, two-dimensional boundary layers.[19–21] In equilibrium boundary layers, velocity-profile similarity scales based on inner and outer boundary-layer variables have been shown to scale high- and low-frequency regions of the surface pressure spectrum, respectively. Additionally, a mixed inner and outer variable scaling has succesfully scaled the low- to middle-frequency range in some cases.[22,23] Recent reviews of the scaling behavior of the pressure power spectrum have been carried out by Keith et al.[24] and Bull.[25] Some uncertainty in the measured behavior have been attributed to the observed Reynolds number dependence of p', limited high-frequency response of transducers due to finite sensing area, and the presence of pressure fluctuations due to nonturbulent sources, that is, acoustics and vibrations.

Surface pressure fluctuations beneath a turbulent boundary layer are related to velocity fluctuations within the boundary layer through a Poisson-type differential equation.[26–28] The Poisson equation may be integrated and shows that surface pressure fluctuations are produced from large regions of the flow. However, the influence of a given source falls off as $1/r_S$.

Much analysis of surface pressure fluctuations beneath equilibrium, two-dimensional boundary layers exists in the literature. The present study extends this knowledge to the analysis of a nonequilibrium, three-dimensional, separating boundary layer of practical interest. Additionally, the flows of the present study cover a large range of Reynolds numbers. Surface pressure–velocity spatial correlation coefficients and the extensive data on the turbulent velocity field are used to explain features of p and p'.

II. Experimental Apparatus and Techniques

The measurements were made in the Virginia Polytechnic Institute and State University Stability Wind Tunnel. This tunnel is a continuous, closed return, subsonic wind tunnel with a 7-m-long and 1.8-m^2 test section. The regulated fan dc power source, a 9:1 area contraction, and seven wire-mesh screens provide low freestream turbulence levels of the order of 0.03%.

The 6:1 prolate spheroid used for these measurements is 1.37 m long and is constructed of a machined fiberglass skin bonded to an aluminum frame. A circumferential trip, consisting of posts 1.2 mm in diameter, 0.7 mm high, and spaced 2.5 mm apart, was placed around the model at $x/L = 0.2$. This fixed the location of transition. Windows of size $30 \times 150 \times 0.75$ mm (Fig. 2) were placed in the skin for optical (LDV) access to the flow.[7,14,15] The windows were molded to the curvature of the model and mounted flush with the model surface to minimize flow disturbances. Wax was used to fill any small gaps in the model surface. The model was supported with a rear-mounted, 0.75-m-long sting aligned along the model axis and connected to a vertical post extended through the wind tunnel floor. All measurements were conducted at a constant Reynolds number, $Re_L = 4.20 \times 10^6$ (50.73 m/s $< U_\infty <$ 55.25 m/s) and ambient temperature.

The pressure transducer used is an Endevco model 8507-C2, which is a circular deflection-type transducer that has a flat frequency response from 0 to 70 kHz. The transducer was mounted inside the model and fixed to one of the windows. The transducer signal was amplified by a Measurements Group model 2310 strain gauge conditioning amplifier.

Access to the flowfield was provided through a 0.5-mm-diam pinhole (Fig. 2). This pinhole and the associated dead volume have a second-order frequency transfer function with a resonant frequency near 12 kHz as shown from calibrations.[29] Contributions of sources that are smaller than the pinhole area are spatially integrated and thereby attenuated. This effect has been investigated,[30–33] and Corcos[30] provides a correction to the wall pressure spectrum in terms of $\omega d/2U_C$, where ω/U_C is the wave number. Schewe[31] found this correction to be adequate for $\omega d/2U_C < 4$. More recently, Lueptow[32] reported that the Corcos[30] correction recovers the true wall pressure spectrum for $\omega d/U_C < 11.0$ for a circular deflection-type transducer such as was used in the present study. Gravante et al.[33] report that the maximum allowable sensing diameter to avoid spectral attenuation at high frequencies is in the range $12 < d^+ < 18$ and that for $d^+ < 27$ the reduction in p' was "barely observable."[33] The pinhole was used to reduce spatial averaging in the present study ($\omega d/2U_C < 0.7$ and $38 < d^+ < 92$). The present flow was nonequilibrium, and neither $U_c(\omega)$ nor the lateral and streamwise spatial coherency of p were measured. Therefore, the Corcos[30] correction was not applied to the spectra presented here. However, p spectra and p' values with the Corcos correction applied may be found in Refs. 29 and 34.

Another difficulty arises in isolating p due to turbulence from p due to other sources. Measured pressure signals are usually contaminated by coherent, facility-related acoustic pressures and external vibration of the transducer. To eliminate these effects a time-delay noise cancellation technique of Agarwal and Simpson[35] was used that relies on the relatively small coherence of turbulent pressure fluctuations in time and space. Here the signal from a single transducer was delayed by the period of a given frequency and subtracted from the original signal, canceling the contributions from coherent sources at that frequency and higher harmonics. The time delay was chosen to be identical to the bin width of the power spectrum

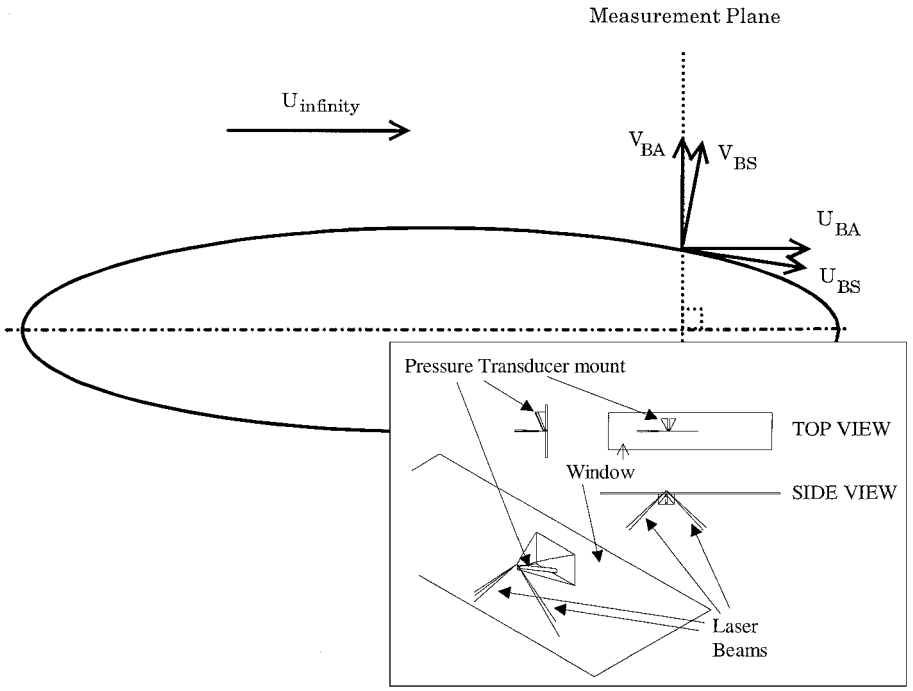

Fig. 2 Relationship between body axis (BA) coordinate system and body surface (BS) coordinate system; insert: schematics of pinhole and cylindrical pressure transducer mount attached to double-convex curvature LDV window.

estimate. In this way, the coherent contributions of sound and vibration are eliminated from each spectral value.

The pressure fluctuations were sampled at 71 kHz with 12-bit precision. This sampling rate is higher than is commonly used. At each location, 25 records of 16,384 data points each were acquired. During postprocessing, each of these contiguous records was divided into subrecords and the time-delay subtraction was carried out. Spectral values were calculated using at least 500 averages. Additional bin averaging was performed to produce the final spectrum.[36] The spectra presented here are single sided.

Velocity measurements for the wall pressure–velocity covariance were made radially and 1 mm windward of the pressure pinhole using a three-orthogonal-velocity-component, fiber-optic LDV probe (55-μm spherical measurement volume) designed specifically for these experiments and described in detail in Ref. 15. The probe is mounted inside the model with all laser beams passing through a window (Fig. 2). It can be remotely traversed ± 2.5 cm in both the axial direction and normal to the major axis of the model. Positioning in the circumferential direction, ϕ, is achieved by rotating the model about its major axis on the sting.

The Doppler frequency of each of the LDV signals was analyzed using three Macrodyne model FDP3100 frequency-domain signal processors operating in coincidence mode. The flow was seeded using polystyrene latex spheres 0.7 μm in diameter. The particle velocity and the pressure at the window pressure tap (Fig. 2) were sampled simultaneously and stored with 16-bit precision. The sample rate varied from 40 samples/s near the surface to 250 samples/s in the outer part of the measurement region.

Boundary-layer velocity profiles were measured at 10–14 circumferential locations from $\phi = 90$ to 180 deg (see Ref. 15). Each profile consisted of 17–19 radial locations from 0.007 cm above the model surface out to 2.5–3.0 cm. At each of these locations 16,384 coincident three-dimensional velocity–surface pressure realizations were acquired.

The surface pressure data acquired simultaneously with the three-dimensional velocity data were used to compute the surface pressure–velocity covariance. They were not used to compute pressure spectra. Separate surface pressure measurements were made at a higher sampling rate (71 kHz) and used to compute the pressure spectra. Pressure fluctuations due to acoustics and vibration do not affect the surface pressure–velocity covariance because only p contributions due to turbulence are related to the turbulent velocity fluctuations.

III. Uncertainty Estimates

The uncertainty in rms velocity fluctuation measurements is within 1.5% (Ref. 15). Note that turbulence quantities at the edge of the boundary layer are limited by a minimum measurable turbulence intensity of about 1.5%. Motion of the LDV probe in the radial direction was achieved by a rotary-encoded servomotor, with repeatability of the radial position of better than $\pm 8\ \mu$m. The circumferential position was measured with a sting-mounted, vernier-type scale and is uncertain to within 0.1 deg. The fiberglass skin of the model followed the nominal prolate spheroid shape to within 0.005 in.

The pressure measurements made simultaneously with velocity were not adjusted for the response of the pressure transducer at high frequencies. In consideration of the rapid decay of the pressure spectrum with frequency and the loss of correlation between surface and interior fluctuations as frequency increases, the uncertainty this introduces in the surface pressure–velocity covariance is very small. The experimental uncertainty for the pressure spectra is ± 1 dB below and ± 2 dB above 11 kHz, including the calibration, finite bandwidth, and finite record length effects.[36] Nearly all of the uncertainty in the pressure spectra was due to frequency response calibration of the pressure transducer. Gravante et al.[33] report that the maximum allowable sensing diameter to avoid spectral attenuation at high frequencies is in the range $12 < d^+ < 18$. To have $d^+ \leq 18$ in the present study would require a pinhole diameter of 0.09 mm which, in turn, would lower the Helmholtz resonant frequency of the pinhole to 1860 Hz ($\omega\nu/u_\tau^2 = 0.07$; $\omega\delta^*/U_e = 0.78$). Such a low resonant frequency would cause significant attenuation of the high-frequency spectral values, thus offsetting any benefit of increased spatial resolution. The uncertainty in p' due to the uncertainty in each spectral estimate is $\pm 1\%$ and is discussed further in Sec. IV.D.

IV. Results and Discussion

A. Mean Flow

The velocity components are presented here as U, V, and W in the body surface coordinate system. This is different from the body axis coordinate system that uses x, r, and ϕ to define a position. The difference is shown in Fig. 2. The transformation from the body axis coordinate system to the body surface coordinate system involves a rotation about the ϕ axis. The rotations required are 1.948 and 6.167 deg at $x/L = 0.600$ and 0.772, respectively. The axial locations $x/L = 0.600$ and 0.772 were chosen for the present study because detailed LDV measurements of the

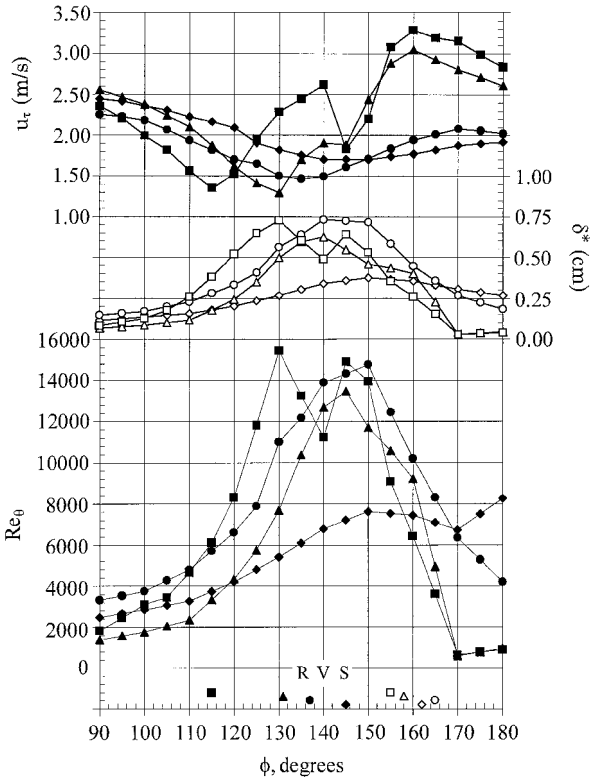

Fig. 3 Variation of displacement thickness δ^*, friction velocity u_τ, and Reynolds number Re_θ with ϕ position: ◇, $\alpha = 10$ deg, $x/L = 0.600$; ○, $\alpha = 10$ deg, $x/L = 0.772$; △ $\alpha = 20$ deg, $x/L = 0.600$; and □, $\alpha = 20$ deg, $x/L = 0.772$; solid symbols immediately above the ϕ axis are location of primary separation,[1] open symbols immediately above the ϕ axis are approximate location of the shed vortex core, and R, V, and S are location of reattachment, secondary vortex core, and secondary separation, respectively, for $\alpha = 20$ deg and $x/L = 0.772$.

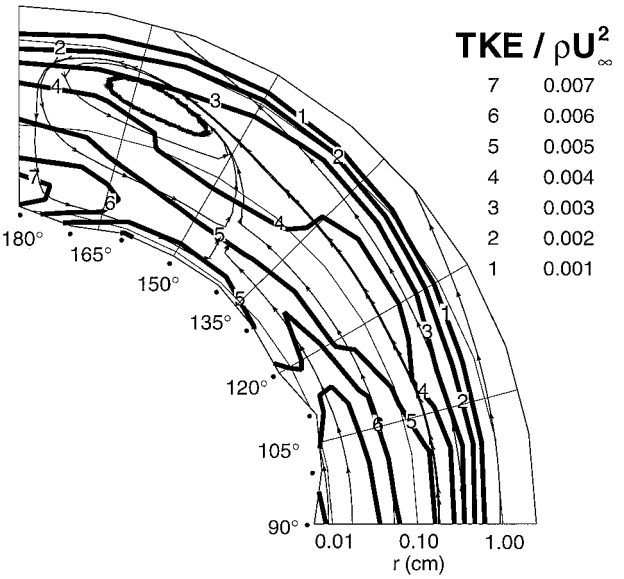

Fig. 4 Secondary streamlines with contour levels of TKE: $\alpha = 10$ deg and $x/L = 0.600$. (Note that the radial coordinate r is plotted on a log scale and that dots denote the azimuthal locations at which radial profiles of simultaneous velocity and surface pressure measurements were made; irregular shape of the inner boundary of each plot is defined by the measurement locations nearest the model surface.)

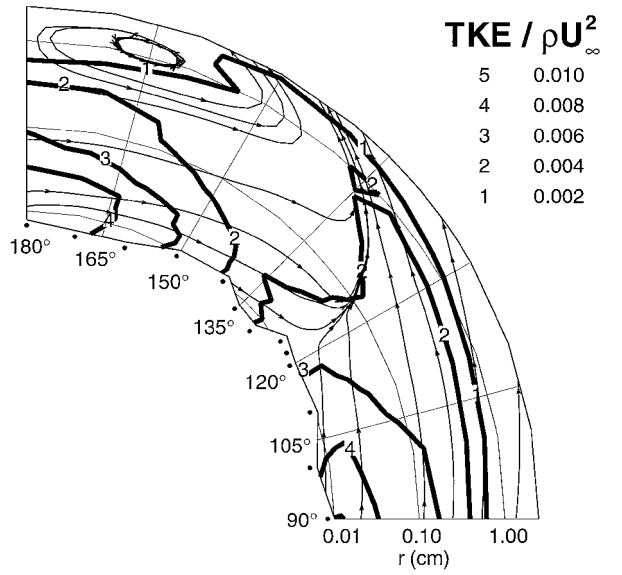

Fig. 5 Secondary streamlines with contour levels of TKE: $\alpha = 10$ deg and $x/L = 0.772$ (see note in caption of Fig. 4).

three-dimensional, crossflow separation are available at these x/L locations.[1,7,13–15]

The mean flow and Reynolds-averaged turbulence stresses have been previously discussed.[7,14,15] Figure 3 shows distributions of u_τ, δ^*, and Re_θ. Mean velocity profiles from LDV measurements and outer layer hot-wire anemometer data[37] were used to calculate δ^* and θ (Ref. 29). The nearest wall region ($y^+ < 50$) of the present flow follows the law-of-the-wall mean velocity profile when expressed in wall shearing stress coordinates.[7,14,15] Figures 4–7 show secondary flow streamlines interpolated from the V and W data for each station. Figures 4–7 also contain contours of the turbulent kinetic energy (TKE) $[\frac{1}{2}\rho(\overline{u^2} + \overline{v^2} + \overline{w^2})]$ to show qualitatively how the mean flowfield and the turbulence field are related.

The secondary flowfield at $\alpha = 10$ deg and $x/L = 0.600$ is shown in Fig. 4. Mean flow separation, as indicated by a minimum in skin-friction magnitude,[1] is at $\phi = 145$ deg, with a vortex center (zero secondary flow velocity) at $\phi = 162$ deg approximately 0.375 cm above the surface. Figure 5 shows the flowfield at $\alpha = 10$ deg and $x/L = 0.772$. Mean flow separation[1] is at $\phi = 137$ deg, with a vortex approximately 1.25 cm above the surface at $\phi = 165$ deg. For each of these $\alpha = 10$ deg cases, the TKE near the wall is maximum at $\phi = 90$ deg and 180 deg because of large production due to large mean velocity gradients and turbulent shear stresses. It decreases in the middle range of ϕ (120–150 deg). However, at any given ϕ location the maximum TKE remains in the near-wall region.

The flowfield at $\alpha = 20$ deg and $x/L = 0.600$ is shown in Fig. 6. Mean flow separation[1] occurs at $\phi = 131$ deg. The separation sheet rolls into a vortex centered at $\phi = 158$ deg, approximately 1.8 cm from the surface. Additionally, at $\phi = 140$ deg there are kinks in the streamlines and high TKE contours extend out into the flow. Flow visualization shows a secondary separation to be incipient at this ϕ location.[1]

Figure 7 shows the flowfield at $\alpha = 20$ deg and $x/L = 0.772$. This case has the highest degree of three dimensionality of the cases considered here. The primary separation[1] location has moved down to $\phi = 115$ deg and the primary vortex has moved outside the LDV measurement region. Hot-wire data show this vortex center to be at $r = 3$ cm, $\phi = 155$ deg (Ref. 37). In addition, a fully formed secondary vortex can be seen at $\phi = 140$ deg approximately 0.6 cm from the surface. Associated with this secondary vortex is separation ($\phi = 145$ deg) and reattachment at $\phi = 135$ deg.

The outward secondary flow streamlines near regions of separation in Figs. 4–7 do not appear to agree with the separation locations. The apparent discrepancy is due to the coordinate system used to represent velocity components and is discussed by Wetzel et al.[1] In a coordinate system locally aligned with the separation line, the LDV data show a zero crossflow velocity very close to the local minimum in skin-friction magnitude.[1] The vortices away from the wall have relatively low mean velocity gradients and bring fluid with relatively low TKE from the outer layer toward the wall at the most leeward (highest) ϕ locations.

The mean flow at the $\alpha = 20$ deg stations has a stronger effect on the turbulence field. High TKE is not confined to the near-wall

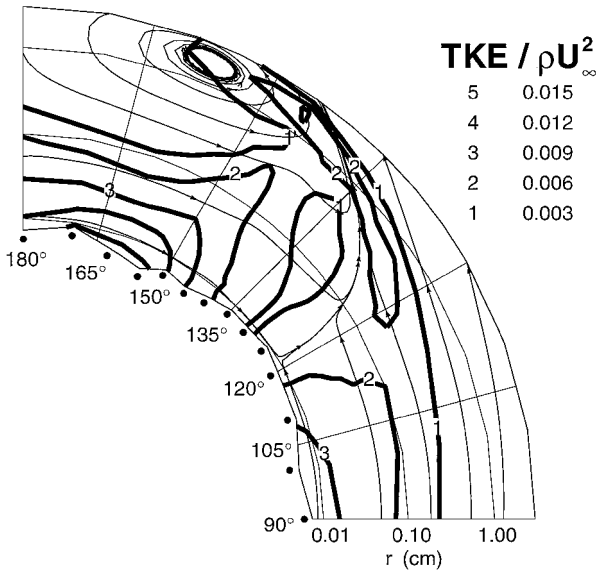

Fig. 6 Secondary streamlines with contour levels of TKE: $\alpha = 20$ deg and $x/L = 0.600$ (see note in caption of Fig. 4).

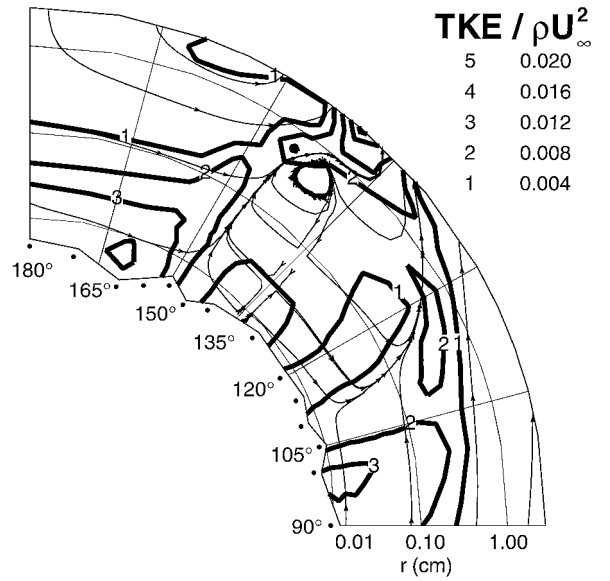

Fig. 7 Secondary streamlines with contour levels of TKE: $\alpha = 20$ deg and $x/L = 0.772$ (see note in caption of Fig. 4).

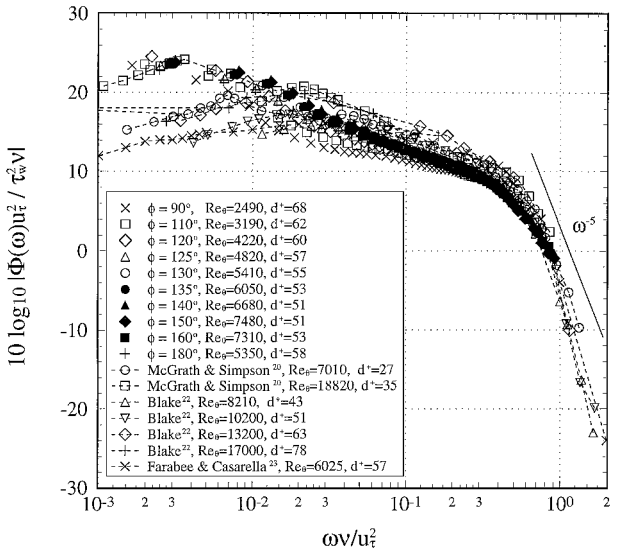

Fig. 8 Power spectra of wall pressure fluctuations scaled on inner shear layer variables (ν/u_τ, u_τ, τ_w): $\alpha = 10$ deg and $x/L = 0.600$.

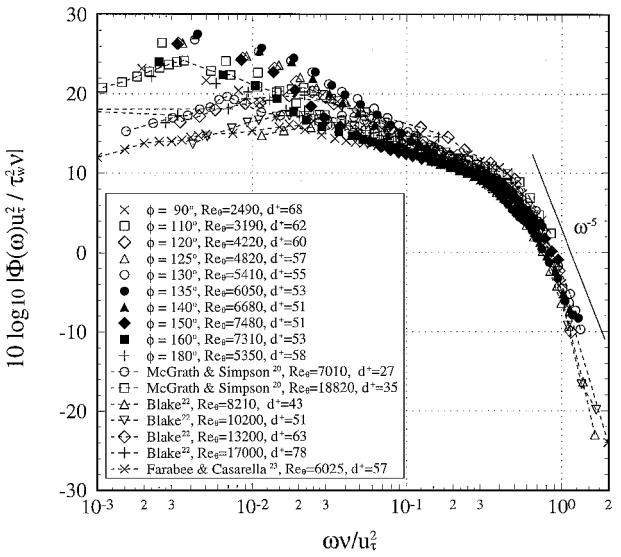

Fig. 9 Power spectra of wall pressure fluctuations scaled on inner shear layer variables (ν/u_τ, u_τ, τ_w): $\alpha = 10$ deg and $x/L = 0.772$.

region. Pockets of highly turbulent fluid appear away from the wall due to the separations. Additionally, each of the separations is followed by low turbulence levels near the wall, and, where reattachment is present, the levels are higher.

B. Surface Pressure Spectra

Surface pressure measurements were carried out at 5-deg increments of ϕ. For clarity, only spectra at about half of the ϕ locations are presented here; the others are presented in Ref. 29. Figures 8 and 9 show p spectra for the $\alpha = 10$ deg stations scaled using u_τ as the velocity scale and ν/u_τ as the length scale. These inner layer scales are those used for the familiar law-of-the-wall mean velocity profile that holds nearest the wall in these flows.

Spectra at both stations collapse at the higher frequencies, $\omega\nu/u_\tau^2 > 0.3$ and approach the ω^{-5} dependence that has been observed beneath two-dimensional boundary layers.[20,26] The present data compare well with other data sets (Figs. 8 and 9), such as those reviewed by Keith et al.[24] The ϕ locations with ω^{-5} regions are those at which u_τ is smallest and ν/u_τ^2 is largest. The source of the ω^{-5} region of the p spectrum is the smallest turbulent structures nearest the wall.

It has been postulated,[19,21,26] using arguments relating the existence of an inner (viscous region) scaling and an outer (largest eddy) scaling within the boundary layer, that an overlap region exists in the p spectrum beneath two-dimensional boundary layers at high Reynolds numbers. Both inner layer and outer layer scaling hold in this overlap region. Bradshaw[19] argued that the p spectrum in this region decreases as ω^{-1}. The low frequency p spectra at $\alpha = 10$ deg and $x/L = 0.600$ (Fig. 10) vary about as ω^{-1} for $0.07 < \omega\delta^*/U_e < 0.3$ when normalized by outer variables (U_e, δ^*, and q_e). The p spectra in the same range at $x/L = 0.772$ do not scale as well using these variables. Although this flow differs from a two-dimensional adverse-pressure-gradient separation, the spectral levels are comparable to those upstream of detachment reported by Simpson et al.[38] (Figs. 10 and 11). In the midfrequency range around $\omega\delta^*/U_e = 2$, the $\omega^{-0.5}$ variation observed by Simpson et al.[38] is also present.

The variation of the p spectra in the midfrequency range may be a Reynolds number effect. The low-frequency spectral contributions are from the largest shear layer structures. The power spectral contribution of these large structures increases with Reynolds number. The high-frequency scaling is Reynolds number independent. This requires a greater decay in the power spectrum within the midfrequency range as Reynolds number increases.

Figures 12 and 13 show the p spectra for the $\alpha = 20$ deg stronger separation cases. None of the outer variable scalings mentioned earlier make the lower frequencies collapse as well as they roughly do

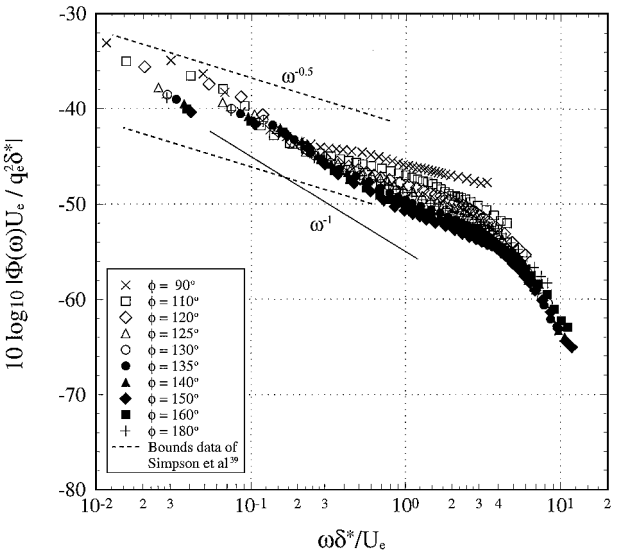

Fig. 10 Power spectra of wall pressure fluctuations scaled on outer shear layer scales (δ^*, U_e, q_e): $\alpha = 10$ deg and $x/L = 0.600$.

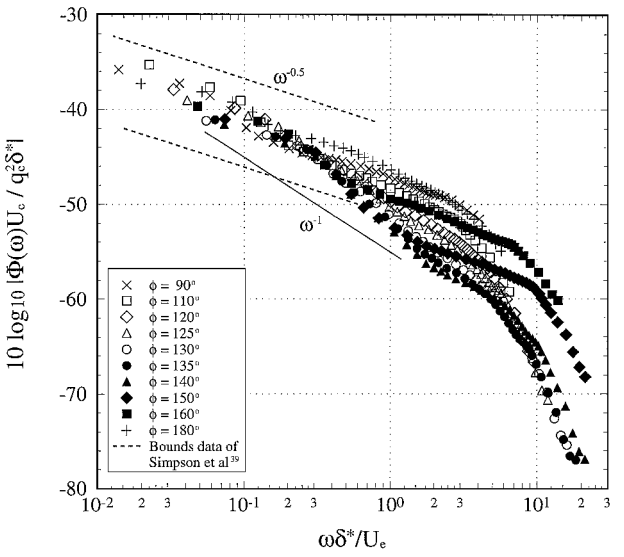

Fig. 11 Power spectra of wall pressure fluctuations scaled on outer shear layer scales (δ^*, U_e, q_e): $\alpha = 10$ deg and $x/L = 0.772$.

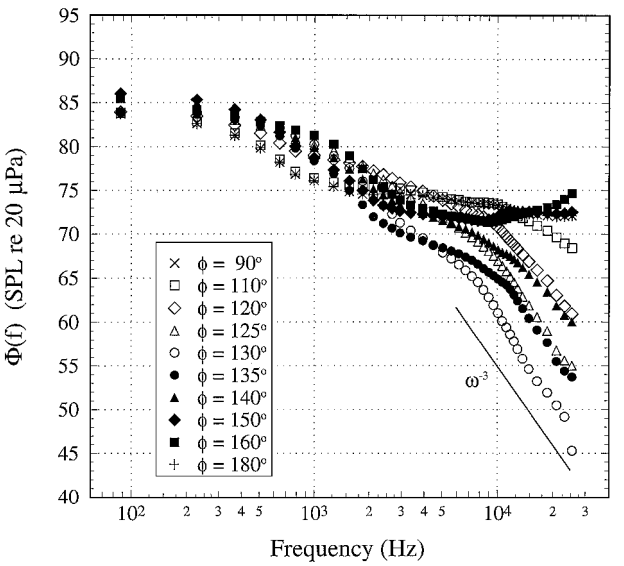

Fig. 12 Power spectra of wall pressure fluctuations: $\alpha = 20$ deg and $x/L = 0.600$.

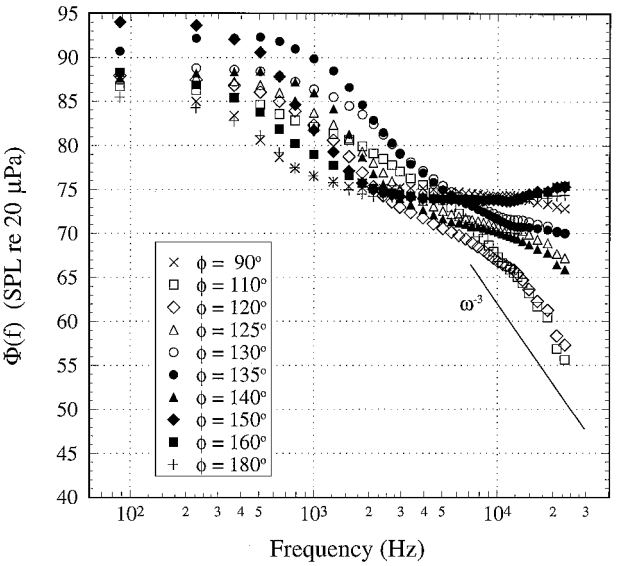

Fig. 13 Power spectra of wall pressure fluctuations: $\alpha = 20$ deg and $x/L = 0.772$.

for the $\alpha = 10$ deg data.[29,34] For $x/L = 0.600$ at 1 kHz, the spectral value has three local maxima: one at $\phi = 130$ deg that is near primary separation, one at $\phi = 145$ deg that is near incipient secondary separation, and one at $\phi = 160$ deg that is near the ϕ location of the center of the shed vortex. The spectral value increases with increasing ϕ to primary separation and decreases with increasing ϕ for $160 \leq \phi \leq 180$ deg. For $x/L = 0.772$ at 1 kHz, the spectral value increases with ϕ to reattachment near $\phi = 135$ deg and then decreases toward the leeward plane of symmetry ($\phi = 180$ deg).

At $x/L = 0.600$, around the primary separation and at windward locations, for $110 < \phi < 135$ deg, there is a strong collapse of spectral content in $\Phi(\omega)U_e/\tau_w^2\delta^*$ vs $\omega\delta^*/U_e$ outer variables for $2 < \omega\delta^*/U_e < 10$ with a ω^{-3} variation.[29] Simpson et al.[38] also observed a ω^{-3} variation during two-dimensional detachment and downstream. However, those spectral levels (using $\tau_{\max}$ instead of τ_w) were about 10 dB below the present levels of -10 dB at $\omega\delta^*/U_e = 10$. At $x/L = 0.772$, around the primary separation[1] $110 < \phi < 120$ deg, an ω^{-3} variation is also observed, but only near $\omega\delta^*/U_e = 10$. For the highest frequencies at locations around the primary separations, u_τ is small enough for the measured spectra to approach $\omega\nu/u_\tau^2 = 1$ and show wall scaling.

Even though the $\alpha = 20$ deg case is a highly nonequilibrium flow, there are some p spectral features that can be consistently related to the flow just discussed. As the flow moves from the windward to leeward sides ($\phi = 90$ deg), there is low-level, low-frequency, large-scaled turbulence content due to the thin accelerating boundary layer with low mean velocity gradients in the outer layer. Substantial high frequency ($\omega \sim u_\tau^2/\nu$) content is produced by the nearest wall-layer structure with a relatively large u_τ. The midfrequencies (4 kHz $< f <$ 10 kHz) have nearly constant, or flat, spectral values.

At more leeward locations the low-frequency content increases because of the thickening boundary layer and the separation with large-scale structures while the high-frequency content is much lower because of much lower u_τ. Farther leeward under the large vortex, the low-frequency content decreases because there are low mean velocity gradients in the outer layer, whereas much larger u_τ values increase the high-frequency content. Again, the midfrequencies have nearly constant spectral values. Note that the spectra for the $\phi = 90$ and 180 deg locations are nearly identical.

The flat midfrequency spectral region is believed to occur because of 1) the lack of overlapping frequency structure between the larger-scale motions and the viscous-dominated region and 2) the decrease of low-frequency content with a substantial increase in the high-frequency levels. The first reason may be due to the three-dimensional flow structure where the near-wall and outer layer flows have different flow histories and low spatial correlations. The second reason just reflects the need for a flatter spectrum to connect the low- and high-frequency contributions.

C. Surface Pressure–Velocity Correlations

To examine the locations of turbulent flow that strongly influence p, simultaneous p and velocity fluctuation measurements were made for three of the stations: $\alpha = 10$ deg, $x/L = 0.772$; $\alpha = 20$ deg, $x/L = 0.600$; and $\alpha = 20$ deg, $x/L = 0.772$. Only distributions of R_{pv} are shown here because the Poisson equation for this flow indicates a strong relationship between p and v. All correlation coefficients (R_{pu}, R_{pv}, R_{pw}) for each station can be found in Ref. 29. Measured surface pressure–velocity covariances for the vicinity of $y^+ = 10$ are expected to be low because of the attenuation of higher frequency surface pressure fluctuations by the pinhole that is much larger than the near-wall coherent structures ($12\nu/u_\tau$).

Figures 14 and 15 show R_{pv} and the fluctuating v-velocity component, respectively, at $\alpha = 10$ deg and $x/L = 0.772$. The maximum negative R_{pv} is from -0.08 to -0.11 at $160 < \phi < 120$ deg, $r \approx 0.1$–0.2 cm, which is roughly at $y^+ \approx 100$–250. Highly turbulent fluid in this case is present mainly near the wall. This maximum negative correlation occurs at the outer edge of the mean velocity profile semilogarithmic region (in wall-shear stress coordinates[7,13–15]). Bradshaw[19] showed that in two-dimensional boundary layers, with both zero and equilibrium adverse pressure gradients, the semilogarithmic region of the mean-flow velocity profile is the source of the overlap region of the pressure spectrum. The magnitude of R_{pv} is high at this radial location because the overlap region of the spectrum is the main contribution to the $\overline{p^2}$ integral for high enough Reynolds number Re_θ (Ref. 19).

The maximum in R_{pv} in the semilogarithmic region of the mean-flow velocity profile can be seen through the solution to the Poisson equation relating surface pressure fluctuations to velocity fluctuations within the boundary layer. Although this solution is an integral over all of the space, the influence of any individual source decreases as $1/r_S$. In contrast, the magnitude of the v' source terms are small for small r_S, where they are constrained by the wall. They increase to a maximum toward the middle of the boundary layer. The combined effect is that the semilogarithmic region is where the strength of source terms are high, and $1/r_S$ is still high enough that these sources influence the pressure at the wall.

Returning to Fig. 14, the high correlation at the edge of the log layer is not evident at all ϕ positions. In the separation region, $120 < \phi < 160$ deg, R_{pv} remains low for all r. However, by considering the behavior of $\overline{v^2}$ (Fig. 15), this is to be expected. A band of maximum v' exists away from the wall in the separation region. Pressure fluctuation sources located farther from the wall have less influence on p.

A layer of large negative R_{pv} is also present at $\alpha = 20$ deg (Fig. 16). However, it is overshadowed by the presence of a localized source. This localized source is associated with the secondary vortex present at $x/L = 0.772$, $r = 0.6$ cm, and $\phi = 140$ deg. Also associated with the secondary vortex is the presence of a secondary separation at $\phi = 145$ deg and reattachment at $\phi = 135$ deg. Here the term localized source is used to describe a small range of r and ϕ in which R_{pv} is high. This particular source is where the secondary flow streamlines have high curvature and the streamwise flow is rapidly decelerating. There is a localized region of high v' at $\alpha = 20$ deg and $x/L = 0.772$ near $r = 1.5$ cm and $\phi = 140$ deg (Fig. 17) that is also a localized source of p. Although this localized source is away from the wall ($y^+ \approx 2200$), the presence of reattachment causes pressure fluctuations associated with this source to be convected to the surface. High negative R_{pv} is observed near this region where high v' and reattachment is present.

D. Mean Square Pressure Fluctuations

Each of the p spectra were integrated to obtain $\overline{p^2}$ values. To use a more complete spectrum, a high-frequency contribution to the mean square integral was added to the numerically integrated experimental spectral estimates. Because the spectra collapse when scaled on inner variables, the high-frequency behavior can be described by a single curve.

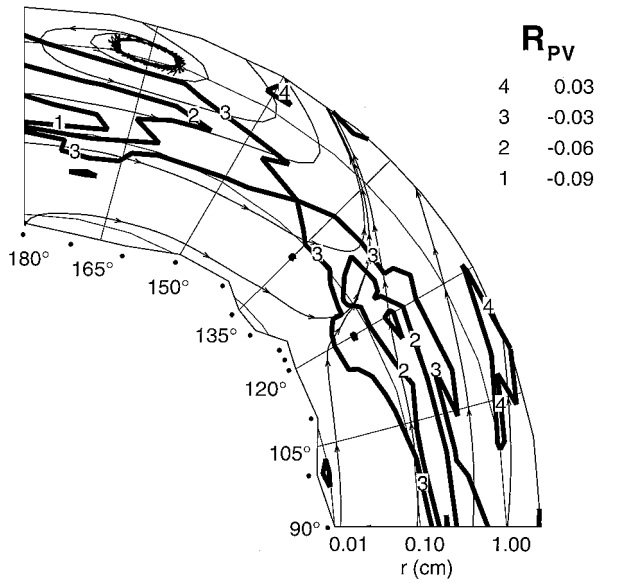

Fig. 14 Secondary streamlines with contour levels of the correlation coefficient R_{pv} of wall pressure and the fluctuating v-velocity component: α = 10 deg and x/L = 0.772 (see note in caption of Fig. 4).

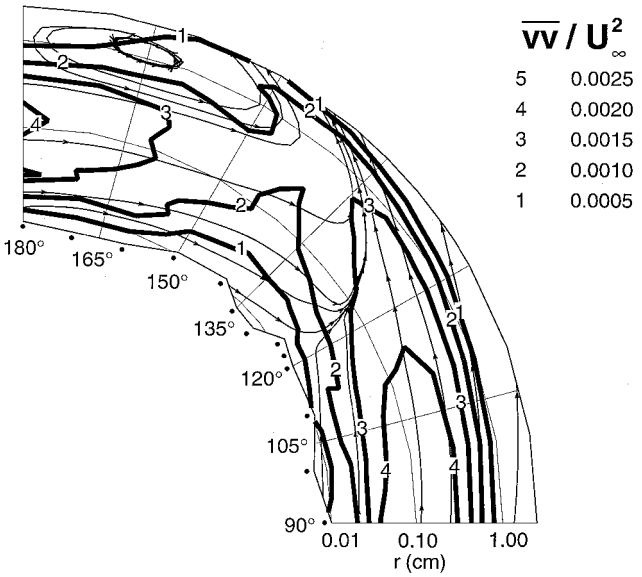

Fig. 15 Secondary streamlines with contour levels of the fluctuating v-velocity component: α = 10 deg and x/L = 0.772 (see note in caption of Fig. 4).

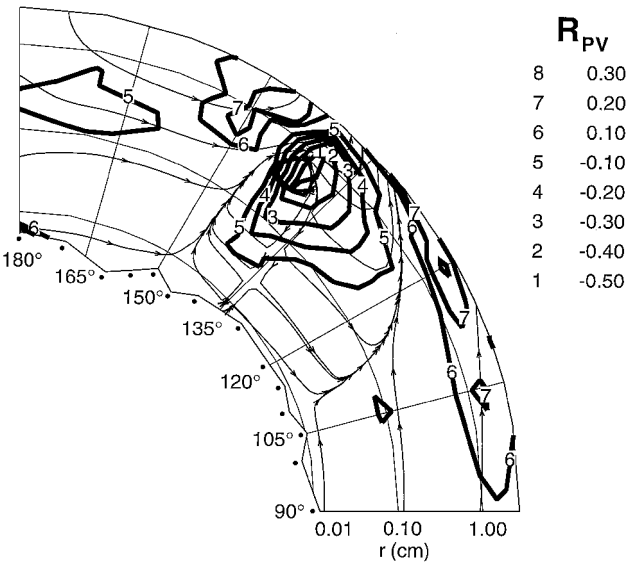

Fig. 16 Secondary streamlines with contour levels of the correlation coefficient R_{pv} of wall pressure and the fluctuating v-velocity component: α = 20 deg and x/L = 0.772 (see note in caption of Fig. 4).

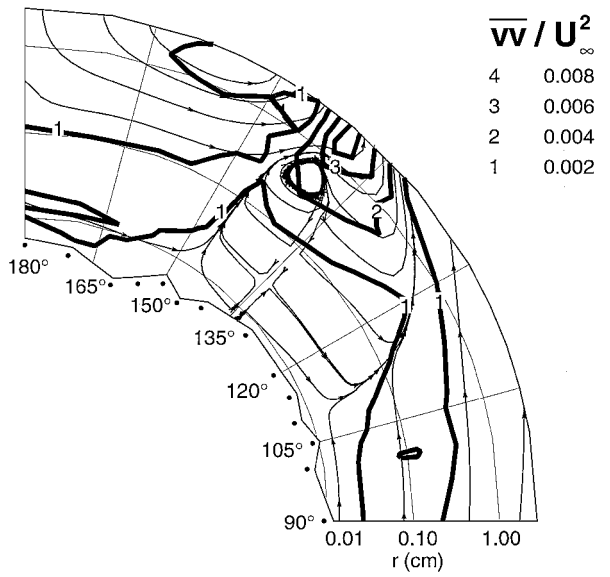

Fig. 17 Secondary streamlines with contour levels of the fluctuating v-velocity component: $\alpha = 20$ deg and $x/L = 0.772$ (see note in caption of Fig. 4).

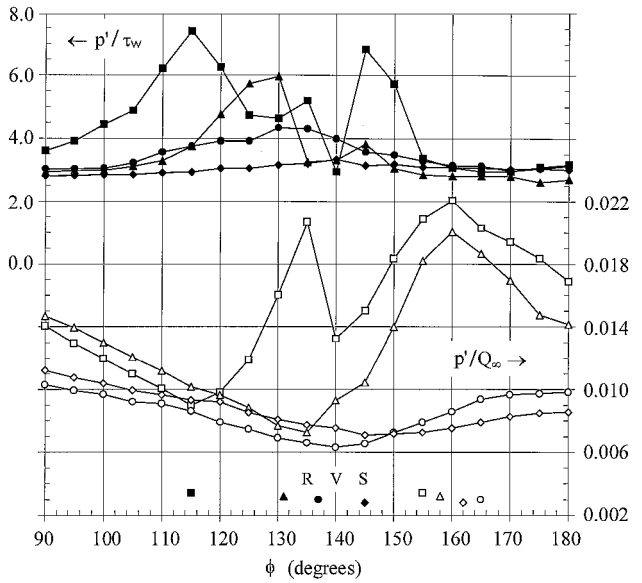

Fig. 18 Variation of rms wall pressure fluctuations with ϕ position: ◇, $\alpha = 10$ deg, $x/L = 0.600$; ○, $\alpha = 10$ deg, $x/L = 0.772$; △ $\alpha = 20$ deg, $x/L = 0.600$; □, $\alpha = 20$ deg, $x/L = 0.772$; solid symbols immediately above the ϕ axis are location of primary separation,[1] open symbols immediately above the ϕ axis are approximate location of the shed vortex core, and R, V, and S are location of reattachment, secondary vortex core, and secondary separation, respectively, for $\alpha = 20$ deg and $x/L = 0.772$.

The procedure used here was to first numerically integrate the experimental spectral estimates. Then the last spectral estimate (highest frequency) was scaled on inner variables. This nondimensional estimate served as the lower limit of an analytical integral, the integrand being proportional to ω^{-5}. Once made dimensional, the value of this analytical integral yields the high-frequency contribution to $\overline{p^2}$.

The p' estimates are shown in Fig. 18 scaled on the far upstream dynamic pressure Q_∞ and scaled on the wall shear stress τ_w. The τ_w is a local minimum at separation.[1] Values of these ratios at $\alpha =$ 10 deg are in the range found for two-dimensional flows.[26,38] A local minimum in p' occurs very close to the separation locations, whereas a local maximum is near the reattachment and under the large vortex center at $\alpha = 20$ deg and $x/L = 0.772$. The p'/τ_w value magnifies the effect of the separation and follows the relative contribution of the outer layer and low-frequency spectral contribution as compared to the viscous wall layer high-frequency contribution. Around the separation locations larger values of p'/τ_w occur because low-frequency contributions are relatively large, whereas τ_w is much lower with a lower contribution from the viscous region.

For $\alpha = 10$ deg, the high-frequency analytical integral contribution (AIC) to p^2 is at most only a few percent of the numerically integrated part. For $\alpha = 20$ deg, the AIC varies from less than 1% of the total p^2 near separation, where p^2 is lowest, to about 44% of the total p^2 at $x/L = 0.600$ and 50% at $x/L = 0.772$ at ϕ locations under the vortex, where p^2 is large. Although the AIC to p^2 is large for some ϕ locations at $\alpha = 20$ deg, note that the values shown in Fig. 18 are a lower bound on the true p' values. Therefore, the variation of p' with ϕ that is shown in Fig. 18 is accurate. At ϕ locations where p' is small, the AIC is small. At ϕ locations where p' large, the AIC is large; however, the true p', if different, is higher than the value reported in Fig. 18. Additionally, the power spectrum at ϕ locations where the AIC is large are nearly flat in the middle- to high-frequency range. The large AIC at these ϕ locations emphasizes the large contribution of the power spectrum at high frequencies to the p^2 integral. Recent measurements by Goody and Simpson[39] of the power spectrum of surface pressure fluctuations in another three-dimensional flow also show nearly constant spectral values at middle frequencies. The spectra reported by Goody and Simpson[39] extend to higher frequencies than the flat spectral region and show that the contribution of the flat spectral region to the p^2 integral can be as high as 40%.

V. Conclusions

Measurements of wall-pressure fluctuation were carried out under the three-dimensional shear layer on the stern leeside of a 6:1 prolate spheroid ($x/L = 0.600$ and 0.772) for a constant Reynolds number of 4.20×10^6 at 10- and 20-deg angles of attack. Pressure fluctuation spectra p' and surface pressure–velocity spatial correlation coefficients were obtained and related to the flowfield structure measured earlier.

The nearest wall region ($y^+ < 100$) at the measured locations in these flows follows the law-of-the-wall mean velocity profile when expressed in wall-shearing-stress coordinates. The wall-shearing-stress magnitude decreases to a local minima at crossflow separation locations and to a large local maxima at reattachments and under vortices. The TKE levels near the wall follow these same trends. The updrafts around the regions of separation carry the TKE away from the wall, whereas secondary reattachments bring some TKE back toward the wall. Outer region mean velocities on the windward side of the primary separation increase continually to the inviscid freestream, but increase and then decrease as r increases within the vortices.

Because the surface pressure fluctuations are related closely to the velocity fluctuation structure and particularly to v through the Poisson equation, R_{pv} shows the influence of outer region flowfield features. Windward of the primary separations and leeward of the primary vortex, relatively large negative levels of R_{pv} occur around $100 < y^+ < 250$ and indicate the strong influence of v in this region. In the outermost part of the measured flowfield, relatively large positive values of R_{pv} occur, especially in the updraft of the primary separation. Negative R_{pv} is large upstream of the formation of the mean flow secondary separation and is very large within the strong secondary separation and reattachment.

The p spectra and p' at low angle of attack are comparable to measurements in equilibrium flows. Around separations with low wall shear stresses, the high-frequency content is small, whereas low-frequency contributions from the outer layer are relatively large. In regions with large surface shearing stresses, the wall region produces strong high-frequency spectral content. At locations with relatively small gradients in the outer region mean velocity distribution, there are smaller low-frequency contributions. Both of these features occur around $\phi = 90$ deg and under the large vortices. Therefore, at these locations spectral values are nearly constant at middle and high frequencies. The resulting p' distributions over the surface reflect the importance of the high-frequency wall region contributions. Around separations there are local minima in p'; around reattachments and under the large vortices there are local maxima in p'.

Acknowledgments

The authors appreciate the support of the Office of Naval Research under Grant N00014-94-1-0092 and Grant N00014-94-1-0802; L. P. Purtell, Program Manager.

References

[1]Wetzel, T. G., Simpson, R. L., and Chesnakas, C. J., "Measurement of Three-Dimensional Crossflow Separation," *AIAA Journal*, Vol. 36, No. 4, 1998, pp. 557–564.

[2]Kreplin, H. P., Vollmers, H., and Meier, H. U., "Wall Shear Stress Measurements on an Inclined Prolate Spheroid in the DFVLR 3m × 3m Low Speed Wind Tunnel," Data Rept. DFVLR 1B 222-84/A33, Göttingen, Germany, 1985.

[3]Kreplin, H. P., and Stäger, R., "Measurements of the Reynolds Stress Tensor in the Three-Dimensional Turbulent Boundary Layer of an Inclined Body of Revolution," *9th Symposium on Turbulent Shear Flow*, Dept. of Mechanical Engineering, Kyoto Univ., Kyoto, Japan, 1993, pp. 2-4-1–2-4-6.

[4]Meier, H. U., Kreplin, H. P., Ländauß er, A., and Baumgarten, D., "Mean Velocity Distributions in Three-Dimensional Boundary Layers Developing on a 1:6 Prolate Spheroid with Natural Transition," Data Rept. DFVLR 1B 222-86/A10, Göttingen, Germany, 1984.

[5]Meier, H. U., Kreplin, H. P., and Ländauß er, A., "Wall Pressure Measurements on a 1:6 Prolate Spheroid in the DFVLR 3m × 3m Low Speed Wind Tunnel ($\alpha = 10°$, $U_\infty = 55$ m/s, Artificial Transition)," Data Rept. DFVLR 1B 222-86/A04, Göttingen, Germany, 1985.

[6]Vollmers, H., Kreplin, H. P., and Meier, H. U., "Separation and Vortical-Type Flow Around a Prolate Spheroid—Evaluation of Relevant Parameters," CP-342, AGARD, 1983.

[7]Chesnakas, C. J., and Simpson, R. L., "Measurements of the Turbulence Structure in the Vicinity of a 3-D Separation," *Journal of Fluids Engineering*, Vol. 118, No. 1, 1996, pp. 268–275.

[8]"Calculation of 3D Separated Turbulent Flows in Boundary Layer Limit," AR-255, AGARD, 1991.

[9]Gee, K., Cummings, R. M., and Schiff, L. B., "Turbulence Model Effects on Separated Flow About a Prolate Spheroid," *AIAA Journal*, Vol. 30, No. 3, 1992, pp. 655–664.

[10]Sung, C. H., Griffin, M. J., Tsai, J. F., and Huang, T. T., "Incompressible Flow Computation of Forces and Moments on Bodies of Revolution at Incidence," AIAA Paper 93-0787, Jan. 1993.

[11]Ahn, S., and Simpson, R. L., "Crossflow Separation on a Prolate Spheroid at Angles of Attack," AIAA Paper 92-0428, Jan. 1992.

[12]Barber, K. M., and Simpson, R. L., "Mean Velocity and Turbulence Measurements of Flow Around a 6:1 Prolate Spheroid," AIAA Paper 91-0255, Jan. 1991.

[13]Chesnakas, C. J., Simpson, R. L., and Madden, M. M., "Three Dimensional Velocity Measurements on a 6:1 Prolate Spheroid at Angle of Attack," Dept. of Aerospace and Ocean Engineering, Virginia Polytechnic Inst. and State Univ., Data Rept. VPI-AOE-202, Blacksburg, VA, Aug. 1993.

[14]Chesnakas, C. J., and Simpson, R. L., "Full Three-Dimensional Measurements of the Crossflow Separation Region of a 6:1 Prolate Spheroid," *Experiments in Fluids*, Vol. 17, No. 1/2, 1994, pp. 68–74.

[15]Chesnakas, C. J., and Simpson, R. L., "A Detailed Investigation of the Three-Dimensional Separation About a 6:1 Prolate Spheroid at Angle of Attack," *AIAA Journal*, Vol. 35, No. 6, 1997, pp. 990–999.

[16]Simpson, R. L., "Turbulent Boundary-Layer Separation," *Annual Review of Fluid Mechanics*, Vol. 21, 1989, pp. 205–234.

[17]Simpson, R. L., "Three-Dimensional Turbulent Boundary Layers and Separation," AIAA Paper 95-0226, Jan. 1995.

[18]Simpson, R. L., "Aspects of Turbulent Boundary-Layer Separation," *Progress in Aerospace Sciences*, Vol. 32, Pergamon, Oxford, 1996, pp. 457–521.

[19]Bradshaw, P., "'Inactive' Motion and Pressure Fluctuations in Turbulent Boundary Layers," *Journal of Fluid Mechanics*, Vol. 30, No. 2, 1967, pp. 241–258.

[20]McGrath, B. E., and Simpson, R. L., "Some Features of Surface Pressure Fluctuations in Turbulent Boundary Layers with Zero and Favorable Pressure Gradients," NASA CR-4051, 1987.

[21]Panton, R. L., and Linebarger, J. H., "Wall Pressure Spectra Calculations for Equilibrium Boundary Layers," *Journal of Fluid Mechanics*, Vol. 65, No. 2, 1974, pp. 261–287.

[22]Blake, W. K., "Turbulent Boundary-Layer Wall-Pressure Fluctuations on Smooth and Rough Walls," *Journal of Fluid Mechanics*, Vol. 44, Pt. 4, 1970, pp. 637–660.

[23]Farabee, M. F., and Casarella, M. J., "Spectral Features of Wall Pressure Fluctuations Beneath Turbulent Boundary Layers," *Physics of Fluids A*, Vol. 3, No. 10, 1991, pp. 2410–2420.

[24]Keith, W. L., Hurdis, D. A., and Abraham, B. M., "A Comparison of Turbulent Boundary Layer Wall-Pressure Spectra," *Journal of Fluids Engineering*, Vol. 114, No. 2, 1992, pp. 338–347.

[25]Bull, M. K., "Wall-Pressure Fluctuations Beneath Turbulent Boundary Layers: Some Reflections of Forty Years of Research," *Journal of Sound and Vibration*, Vol. 190, No. 3, 1996, pp. 299–315.

[26]Blake, W. K., *Mechanics of Flow-Induced Sound and Vibration*, Academic, New York, 1986, pp. 497–595.

[27]Kraichnan, R. H., "Pressure Fluctuations in Turbulent Flow over a Flat Plate," *Journal of the Acoustical Society of America*, Vol. 28, No. 3, 1956, pp. 378–390.

[28]Rotta, J. C., "Turbulent Boundary Layers in Incompressible Flow," *Progress in Aeronautical Sciences*, Vol. 2, Pergamon, Oxford, 1962, pp. 10, 11.

[29]Goody, M. C., "An Experimental Investigation of Pressure Fluctuations in Three-Dimensional Turbulent Boundary Layers," Ph.D. Dissertation, Dept. of Aerospace and Ocean Engineering, Virginia Polytechnic Inst. and State Univ., Blacksburg, VA, 1999.

[30]Corcos, G. M., "Resolution of Pressure in Turbulence," *Journal of the Acoustical Society of America*, Vol. 35, No. 2, 1963, pp. 192–199.

[31]Schewe, G., "On the Structure and Resolution of Wall-Pressure Fluctuations Associated with Turbulent Boundary Layer Flow," *Journal of Fluid Mechanics*, Vol. 134, 1983, pp. 311–328.

[32]Lueptow, R. M., "Transducer Resolution and the Turbulent Wall Pressure Spectrum," *Journal of the Acoustical Society of America*, Vol. 97, No. 1, 1995, pp. 370–378.

[33]Gravante, S. P., Naguib, A. M., Wark, C. E., and Nagib, H. M.,, "Characterization of the Pressure Fluctuations Under a Fully Developed Turbulent Boundary Layer," *AIAA Journal*, Vol. 36, No. 10, 1998, pp. 1808–1816.

[34]Goody, M. C., Simpson, R. L., and Chesnakas, C. J., "Surface Pressure Fluctuations and Pressure–Velocity Correlations Produced by a Separated Flow Around a Prolate Spheroid at Incidence," AIAA Paper 97-0485, Jan. 1997.

[35]Agarwal, N. K., and Simpson, R. L., "A New Technique for Obtaining the Turbulent Pressure Spectrum from the Surface Pressure Spectrum," *Journal of Sound and Vibration*, Vol. 135, No. 2, 1989, pp. 346–350.

[36]Bendat, J. S., and Piersol, A. G., *Random Data: Analysis and Measurement*, 2nd ed., Wiley, New York, 1986, pp. 252–290.

[37]Goody, M. C., Simpson, R. L., Engel, M., Chesnakas, C. J., and Devenport, W. J., "Mean Velocity and Pressure and Velocity Spectral Measurements Within a Separated Flow Around a Prolate Spheroid at Incidence," AIAA Paper 98-0630, Jan. 1998.

[38]Simpson, R. L., Ghodbane, M., and McGrath, B. E., "Surface Pressure Fluctuations in a Separating Turbulent Boundary Layer," *Journal of Fluid Mechanics*, Vol. 177, 1987, pp. 167–186.

[39]Goody, M. C., and Simpson, R. L., "An Experimental Investigation of Surface Pressure Fluctuations Beneath Two and Three-Dimensional Turbulent Boundary Layers," AIAA Paper 99-0608, Jan. 1999.

P. R. Bandyopadhyay
Associate Editor